IEEE Access
Multidisciplinary | Rapid Review | Open Access Journal

IEEE POWER & ENERGY SOCIETY SECTION

Received 2 January 2024, accepted 24 January 2024, date of publication 29 January 2024, date of current version 2 February 2024.

Digital Object Identifier 10.1109/ACCESS.2024.3359408

APPLIED RESEARCH

Dynamic State Estimation of a High-Order Model of Doubly-Fed Induction Generator Using Unscented Kalman Filter

ALIF RAVI RAMADHAN, HUSNI ROIS ALI, (Senior Member, IEEE), AND RONI IRNAWAN, (Senior Member, IEEE)

Department of Electrical and Information Engineering, Universitas Gadjah Mada, Yogyakarta 55281, Indonesia

Corresponding author: Husni Rois Ali (husni.rois.ali@ugm.ac.id)

This work was supported by Token APC IEEE-UGM.

ABSTRACT The utilization of renewable energy in power generation has been increasing in recent years, with the use of wind power sources being the most promising solution for sustainable power generation. The doubly-fed induction generator (DFIG) is one of the most commonly used generators in wind power generation applications, as it offers some technical of advantages. However, the increasing penetration of wind power generation poses tremendous technical challenges in power system operation as this can potentially affect system stability, requiring better control and monitoring schemes. Dynamic state estimation (DSE) offers the ability to achieve this purpose. With respect to this, the present paper proposes a DSE framework on a high-order model of DFIG consisting of 18 states. The method uses the unscented Kalman filter (UKF) which provides an accurate estimate of DFIG states under a strong system non linearity present in the wind turbine system. Furthermore, this paper demonstrates the robustness of the proposed method under different faults and noisy conditions. Finally, the paper also extends the use of UKF to estimate the unknown inputs of a DFIG system, such as control references in the rotor-side converter (RSC) and grid-side converter(GSC).

INDEX TERMS Doubly fed induction generator, dynamic state estimation, power system monitoring, unscented Kalman filter, wind power generation.

I. INTRODUCTION

The growing concern on the availability of fossil fuels such as gas and coal and their impact on environmental has led to the increasing utilization of renewable energy sources in power generation. As a result, the current structure of power systems has been transforming into an increasing deployment of renewable energy based power generation, such as wind power and photovoltaic (PV). Due to its abundant availability, cost-effective reasons, and scalability [1], [2], wind energy is considered as one of the most promising solutions for a sustainable power generation. However, the increase in penetration of wind power generation poses tremendous technical challenges in power system operation due to its pertinent intermittent behaviors [3], [4], [5]. A doubly-fed induction generator (DFIG)-based wind turbine is one of the most favorable and commonly used in wind power generation applications as it benefits from variable speed operation capabilities, which reduces mechanical stress and posses a better power capture [6], [7]. In addition, the ability to independently control active and reactive power is another advantage of DFIG [8]. These technical advantages lead to an increasing number of DFIGs integration into power systems, which may adversely affect system stability [9], [10].

Maintaining generator stability plays an important role in ensuring safe and stable operation of power systems. This is increasingly challenging due to the fact that more and more wind power plants have been interconnected to power systems. This condition necessities a better control and monitoring schemes. A dynamic state estimation (DSE) can provide a significant role to serve this purpose. This is

The associate editor coordinating the review of this manuscript and approving it for publication was Feng Wu.

© 2024 The Authors. This work is licensed under a Creative Commons Attribution-NonCommercial-NoDerivatives 4.0 License.
For more information, see https://creativecommons.org/licenses/by-nc-nd/4.0/

possible as DSE allows estimation of internal states of a generator from terminal measurements such as voltage or output power [11]. With this ability, monitoring, control, protection, and assessment of power system stability are enhanced as the internal states can be attributed to system stability [12], [13], [14].

The extended kalman filter (EKF), unscented kalman filter (UKF), and particle filter (PF) are probably the most popular DSE methods applied in power systems. Related studies on synchronous generators (SG) using EKF [15], UKF [16], and PF [17] shows that these methods have been able to provide an accurate estimate of SG states such as rotor speed and angle. This indicates that the methods are applicable to DSE in power generation. References [16], [18], and [19] have performed a comparative study of some DSE methods. The linearization-free methods, namely UKF and PF, have shown better results with higher accuracy than their linearization-based counterparts, namely EKF. The linearization process used in EKF leads to various difficulties [16] such as truncation error [18]. Comparing the estimation results of linearization-free methods under various conditions, [19] shows that PF is able to provide estimates with significantly accuracy than those in UKF, although it is shown that PF may fail to converge in some particular cases. The PF method also normally requires higher number of sample points, known as particles, to produce higher accuracy estimations, resulting in a significantly demanding computational burden.

Previous research has also demonstrated the ability of those DSE methods to be implemented in wind turbine systems for various purposes, such as monitoring [20], control [21], and fault diagnosis [22]. The results from those research have demonstrated that the techniques are also applicable to wind turbine systems. As also observed in the case of synchronous generators, Ref. [23] has shown that the EKF is outperformed by the other linearization-free methods such as UKF for estimating the states of doubly-fed induction generators (DFIG) due to strong non-linearity present in the case of wind turbine systems. Furthermore, obtaining the Jacobin matrix in EKF is often a cumbersome effort, especially in the case of a DFIG as it is normally a high-order system. As a result, linearization-free DSE methods are often preferred for DFIG state estimation. The work presented in [2] and [23] shows that PF results in state estimation with higher degree of accuracy than those in UKF, but again it demands a significantly higher computational cost. This is due to the fact that PF requires a large number of particles to attain accurate results. In contrast to PF, UKF uses a fixed set of deterministic sample point to perform a non-linear estimation. The work in [24] shows that PF experienced escalating computing time while UKF maintain stable computing time, highlighting the UKF's advantage in computational efficiency compared to PF. The work carried out by [2], [21], and [23] has successfully presented DFIG state estimation using UKF. However, the model of DFIG is merely represented by using 6 or 11 states, which may be inadequate to capture the behaviours of DFIG in response to a large disturbance. Furthermore, the issue related to unknown control inputs in the rotor-side converter (RSC) and grid-side converter (GSC) controllers has not been addressed. References [25], [26], and [27] have demonstrated the feasibility of utilizing the kalman filtering methods in unknown input scenarios.

With regards to the above mentioned problem, this paper proposes a DSE application on DFIG-based wind turbines to acquire an accurate estimate of the non-measurable state variables using UKF method [28]. The contributions of the paper are as follows:

1) The state estimate is conducted on an highly nonlinear DFIG system modelled with 18 states. This high order allows for a detailed representation of its dynamics, and hence a better dynamic representation of wind turbine during a large transient event, enhancing the accuracy in analyzing transient events to better reflect real-world conditions.
2) The state estimation framework is decentralized and only requires terminal measurements of DFIGs such as terminal voltage and current, or active and reactive output powers. This decentralized approach is hence expendable to any configurations of DFIG such as stand-alone or grid-connected.
3) The robustness of the proposed method is investigated against some realistic conditions, such as different level of fault severity and different level of process and measurement noises.
4) The ability of UKF is extended to estimate unknown control inputs. This may be beneficial since some variables may be unknown or hard to measure in some specific configurations and cases.

The reminder of this paper is organized as follows. The mathematical model of DFIG dynamics is discussed in Section II. Section III provides a self-contained discussion on UKF algorithm. In Section V, the simulation results of several study cases on DFIG state estimation, including voltage drops, various noise conditions, and unknown inputs, are presented. Finally, Section VI outlines the key findings of this paper.

II. DFIG MATHEMATICAL MODEL

The DFIG mathematical model considered in this paper is derived from [29]. Fig. 1 shows the illustration of the system. As can be seen this is a single DFIG connected to the infinite bus via a series compensated line. While our study is focused on a grid-connected DFIGs, the techniques and approaches proposed in this paper can be extended to both standalone and grid-connected systems, provided the system inputs and outputs are carefully selected. It will be discussed in detail in Section IV. The system parameters are provided in Appendix VI.

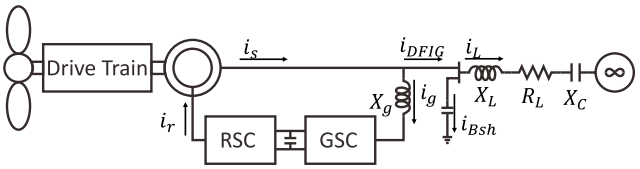

FIGURE 1. Illustration of the study system.

A. SERIES COMPENSATED LINE MODEL

The dynamics of series compensated line in the synchronous reference frame is described as follows.

$$\begin{bmatrix} \dot{v}_{cq} \\ \dot{v}_{cd} \\ \dot{i}_{qL} \\ \dot{i}_{dL} \end{bmatrix} = \omega_b \begin{bmatrix} 0 & -\omega_s & X_c & 0 \\ \omega_s & 0 & 0 & X_c \\ 0 & 0 & -\dfrac{R_L}{X_L} & -\omega_s \\ 0 & \dfrac{-1}{X_L} & \omega_s & -\dfrac{R_L}{X_L} \end{bmatrix} \begin{bmatrix} v_{cq} \\ v_{cd} \\ i_{ql} \\ i_{dl} \end{bmatrix} + \omega_b \begin{bmatrix} 0 \\ 0 \\ \dfrac{v_{qs} - E_{Bq}}{X_L} \\ \dfrac{v_{ds} - E_{Bd}}{X_L} \end{bmatrix} \tag{1}$$

where $i_L = i_{qL} - j i_{dL}$ is the current flowing through the series compensated line.The subscripts d and q refer to the respective variables referred on the direct and the quadrature axis, respectively. E_b is the voltages of the infinite bus, v_c is the voltages across the capacitor, and v_s is the voltages in the DFIG terminal. ω_b and ω_s are the base speed and the synchronous reference speed, respectively.

B. TERMINAL VOLTAGE MODEL

The terminal voltage v_s is affected by the balance between the current injection by DFIG, namely $i_s + i_g$, and the series compensated line current, i_L. This can be described by (2) as follows:

$$\begin{bmatrix} \dot{v}_{qs} \\ \dot{v}_{ds} \end{bmatrix} = \omega_b \begin{bmatrix} 0 & -\omega_s \\ \omega_s & 0 \end{bmatrix} \begin{bmatrix} v_{qs} \\ v_{ds} \end{bmatrix} + \begin{bmatrix} \dfrac{\omega_b}{B_{sh}} & 0 \\ 0 & \dfrac{\omega_b}{B_{sh}} \end{bmatrix} \begin{bmatrix} i_{qBsh} \\ i_{dBsh} \end{bmatrix} \tag{2}$$

where $i_{Bsh} = (i_s - i_g) - i_L$ is the current across the shunt capacitor B_{sh}.

C. DRIVE-TRAIN MODEL

The drive-train is modeled as a two-mass system described by (3) as follows:

$$\begin{bmatrix} \dot{\omega}_t \\ \dot{\omega}_r \\ \dot{T}_g \end{bmatrix} = \begin{bmatrix} \dfrac{D_t - D_{Tg}}{2H_t} & \dfrac{D_{Tg}}{2H_t} & \dfrac{-1}{2H_t} \\ \dfrac{D_{Tg}}{2H_g} & \dfrac{D_t - D_{Tg}}{2H_g} & \dfrac{1}{2H_g} \\ K_{Tg}\omega_s & -K_{Tg}\omega_s & 0 \end{bmatrix} \begin{bmatrix} \omega_t \\ \omega_r \\ T_g \end{bmatrix} + \begin{bmatrix} \dfrac{1}{2H_t} & 0 & 0 \\ 0 & \dfrac{-1}{2H_g} & 0 \\ 0 & 0 & 1 \end{bmatrix} \begin{bmatrix} T_m \\ T_e \\ 0 \end{bmatrix} \tag{3}$$

where T_m and T_e denote the mechanical torque working on the turbine blades and the electrical torque in the generator, respectively. ω_t and ω_r indicate the turbine and the rotor speed, respectively, and T_g is the internal torque of the model. H_t and H_g are the inertia constants of the turbine and the generator respectively. D_t, D_g, and D_{Tg} are the damping coefficients of the turbine, generator, and the shaft coupling connecting the two masses. K_{Tg} is the shaft stiffness coefficient.

D. INDUCTION GENERATOR MODEL

The induction generator can be described as a 6th order dynamical model as discussed in [29]. However, assuming that the DFIG operates in balance, the zero axis current is equal to 0 and can be ignored. Therefore, the induction generator can be model with 4 states as described by the equation as follows.

$$\dot{x}_{gen} = \mathbf{A}_{gen} x_{gen} + \mathbf{B}_{gen} u_{gen} \tag{4}$$

$$\mathbf{B}_{gen} = \begin{bmatrix} \dfrac{-X_s}{\omega_b} & 0 & \dfrac{X_m}{\omega_b} & 0 \\ 0 & -\dfrac{X_s}{\omega_b} & 0 & \dfrac{X_m}{\omega_b} \\ -\dfrac{X_m}{\omega_b} & 0 & \dfrac{X_r}{\omega_b} & 0 \\ 0 & -\dfrac{X_m}{\omega_b} & 0 & \dfrac{X_r}{\omega_b} \end{bmatrix}^{-1} \tag{5}$$

$$\mathbf{A}_{gen} = -\mathbf{B}_{gen} \begin{bmatrix} -r_s & -\omega_s X_s & 0 & \omega_s X_m \\ \omega_s X_s & -r_s & -\omega_s X_m & 0 \\ 0 & -sX_m & r_r & sX_r \\ sX_m & 0 & -sX_r & r_r \end{bmatrix} \tag{6}$$

where $s = 1 - \omega_r$ is the slip. $x_{gen} = \begin{bmatrix} i_{qs} & i_{ds} & i_{qr} & i_{dr} \end{bmatrix}^T$. $u_{gen} = \begin{bmatrix} v_{qs} & v_{ds} & v_{qr} & v_{dr} \end{bmatrix}^T$. i_s and i_r denote the stator and rotor currents, respectively. v_r indicates the rotor voltage.

E. DFIG CONTROL MODEL

In this paper, the rotor side controller (RSC) and grid side controller (GSC) are modeled as cascaded control loop with cross-couplings as given in Figs. 2 and 3, respectively. As can be seen, the outer loop of RSC controls the electromagnetic torque T_e for the maximum power point tracking (MPPT) algorithm and the stator reactive power Q_s, whereas the outer loop of GSC regulates the DC-link voltage V_{DC} and the GSC filter reactive power Q_g.

The differential equations governing the dynamic of RSC are as follows

$$\begin{aligned} \dot{\Phi}_{T_e} &= T_{eref} - T_e \\ \dot{\Phi}_{Q_s} &= Q_{sref} - Q_s \\ \dot{\Phi}_{i_{qr}} &= K_{pT_e}(T_{eref} - T_e) + K_{iT_e}\Phi_{T_e} - i_{qr}^c \end{aligned}$$

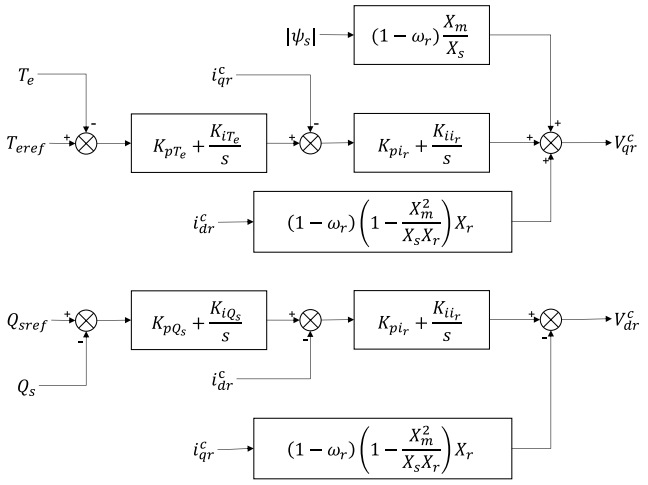

FIGURE 2. RSC control loop.

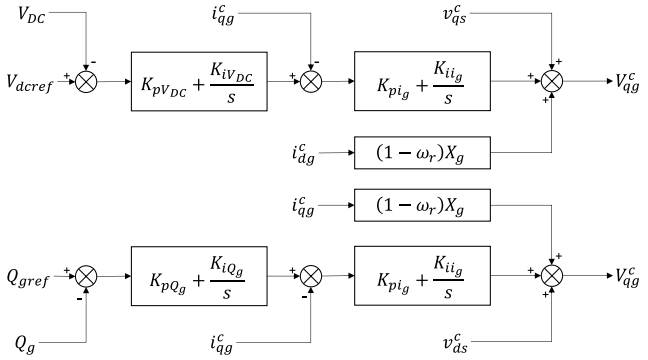

FIGURE 3. GSC control loop.

$$\dot{\Phi}_{i_{dr}} = K_{pQ_s}(Q_{sref} - Q_s) + K_{iQ_s}\Phi_{Q_s} - i_{dr}^c \tag{7}$$

$K_{pT_e}, K_{iT_e}, K_{pQ_s}$ and K_{iQ_s} refer to the constants in the RSC PI controllers. $i_r^c = i_{qr}^c - ji_{qr}^c = i_r e^{j\theta}$ with $\theta = \tan^{-1}(-v_{qs}/v_{ds})$ denotes the rotor current referred to the control reference frame. Further, the differential equations governing the dynamic of GSC are expressed as follows

$$\begin{aligned}
\dot{\Phi}_{V_{DC}} &= V_{DCref} - V_{DC} \\
\dot{\Phi}_{Q_g} &= Q_{gref} - Q_g \\
\dot{\Phi}_{i_{qr}} &= K_{pV_{DC}}(V_{DCref} - V_{DC}) + K_{iV_{DC}}\Phi_{V_{DC}} - i_{qg}^c \\
\dot{\Phi}_{i_{dg}} &= K_{pQ_g}(Q_{gref} - Q_g) + K_{iQ_g}\Phi_{Q_g} - i_{dg}^c
\end{aligned} \tag{8}$$

$K_{pV_{DC}}, K_{iV_{DC}}, K_{pQ_g}$ and K_{iQ_g} refer to the constants in the GSC PI controllers. $i_g^c = i_{qg}^c - ji_{qg}^c = i_g e^{j\theta}$ indicates the GSC filter current referred to the control reference frame.

F. GSC FILTER

The GSC filter current i_g is affected by the voltage difference between GSC and the terminal. Eqn. (9) describes the dynamics of i_g.

$$\begin{bmatrix} \dot{i}_{qg} \\ \dot{i}_{dg} \end{bmatrix} = \begin{bmatrix} \frac{X_g}{\omega_b} & 0 \\ 0 & \frac{X_g}{\omega_b} \end{bmatrix}^{-1} \begin{bmatrix} 0 & \omega_s X_g \\ -\omega_s X_g & 0 \end{bmatrix} \begin{bmatrix} i_{qg} \\ i_{dg} \end{bmatrix} + \begin{bmatrix} \frac{X_g}{\omega_b} & 0 \\ 0 & \frac{X_g}{\omega_b} \end{bmatrix} \begin{bmatrix} \Delta v_{sq} \\ \Delta v_{sd} \end{bmatrix} \tag{9}$$

where X_g shows the filter reactance. $\Delta v_{sq} = v_{gq} - v_{sq}$ and $\Delta v_{sd} = v_{gd} - v_{sd}$ denote the voltage difference between GSC output and DFIG terminal.

G. DC-LINK MODEL

The RSC and GSC are connected by the DC-link, which acts as a temporary evergy storage. The nonlinear dynamics of a DC-link capacitor voltage can be described by (10) as follows.

$$C_{V_{DC}} V_{DC} \frac{\mathrm{d}V_{DC}}{\mathrm{d}t} = P_r - P_g \tag{10}$$

where $C_{V_{DC}}$ and V_{DC} refer to the DC-link capacitor and its corresponding voltage, respectively. $P_g = \frac{1}{2}(v_{qg}i_{qg} + v_{dg}i_{dg})$ and $P_g = \frac{1}{2}(v_{qg}i_{qg} + v_{dg}i_{dg})$ indicate the power flowing from the rotor and into the GSC filter, respectively.

III. UNSCENTED KALMAN FILTER

The Unscented Kalman Filter is a method to estimate the dynamic states of a nonlinear system by utilizing the unscented transformation (UT). UT was developed to transform mean and covariance of a variable through nonlinear transformation overcoming deficiencies of linearization used in other method such as the Extended Kalman Filter [30]. A set of sample points, also called sigma points, are chosen to estimate statistical properties of a distribution through a nonlinear transformation. UT is illustrated in Fig. 4.

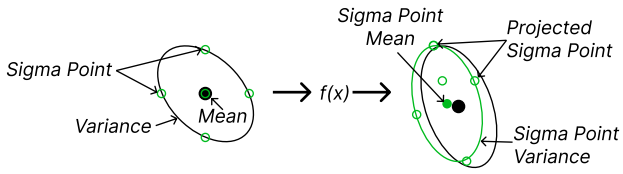

FIGURE 4. Illustration of unscented transformation.

A. SIGMA POINTS

Sigma points are selected in a deterministic step in order to capture accurately statistical information. The sigma points selection proposed in [31] is adopted in this paper. Suppose x is a normally distributed L dimension vector with mean $\hat{x}$ and covariance $\mathbf{P}_x$, a total of $2L+1$ sigma points χ are chosen according to (11)-(13).

$$\chi_0^x = \bar{x} \tag{11}$$

$$\chi_i^x = \bar{x} + (\sqrt{(L+\lambda)\mathbf{P}_x})_i \,, \quad i = 1, \ldots, L \tag{12}$$

$$\chi_i^x = \bar{x} - (\sqrt{(L+\lambda)\mathbf{P}_x})_i \,, \quad i = L+1, \ldots, 2L \tag{13}$$

$\lambda = \alpha^2(L+\kappa) - L$ gives the scaling parameter. α denotes a small positive number usually smaller than 1. The secondary scaling parameter κ is usually set to 0.

Adding the weight to each sigma point can reduce approximation error by performing a weighted average on the UT process. The weight for each sigma point can be calculated according to (14)-(16). $W^{(m)}$ and $W^{(c)}$ are weights for mean and covariance calculations, respectively.

$$W_0^{(m)} = \frac{\lambda}{L+\lambda} \tag{14}$$

$$W_0^{(c)} = \frac{\lambda}{L+\lambda} + (1 - \alpha^2 + \beta) \tag{15}$$

$$W_i^{(m)} = W_i^{(c)} = \frac{1}{2(L+\lambda)} \tag{16}$$

β is the degree of freedom and its value is set to 2 for the normal distribution.

B. UNSCENTED KALMAN FILTER ALGORITHM

The unscented kalman filter discussed in [31] will be used in this paper. The UKF algorithm will be described for a discrete nonlinear system with the process equation shown as (17) and the measurement equation shown as (18). The process $\mathbf{v}$ and measurement noises $\mathbf{w}$ are both assumed to be normally distributed.

$$\mathbf{x}_k = f(\mathbf{x}_{k-1}, \mathbf{u}_{k-1}) + \mathbf{v}_k \tag{17}$$

$$\mathbf{y}_k = g(\mathbf{x}_k) + \mathbf{w}_k \tag{18}$$

where $\mathbf{v}_k \sim \mathcal{N}(0, Q_k)$, $\mathbf{w}_k \sim \mathcal{N}(0, R_k)$.

UKF consist of two main steps, namely the time update and measurement update. Prediction is acquired in time update step, whereas the refined using actual measurement in measurement update step. Initial state estimation $\hat{\mathbf{x}}_0$ and the corresponding covariance $\mathbf{P}_0^x$ are required to initialize UKF state estimation.

In the time update step, the prediction is acquired by generating sigma points and transforming them through the process model shown as (19). These transformed sigma points can be used to calculate the prediction $\hat{\mathbf{x}}_k^-$ and the respective covariance $\mathbf{P}_k^{x-}$ according to (20) and (21).

$$\chi_{k|k-1}^x = f(\chi_{k-1|k-1}^x, \mathbf{u}_{k-1}) \tag{19}$$

$$\hat{\mathbf{x}}_k^- = \sum_{i=0}^{2L} \mathbf{W}_i^{(m)} \chi_{i,k|k-1}^x \tag{20}$$

$$\mathbf{P}_k^{x-} = \sum_{i=0}^{2L} \mathbf{W}_i^{(c)} (\chi_{i,k|k-1}^x - \hat{\mathbf{x}}_k^-)(\chi_{i,k|k-1}^x - \hat{\mathbf{x}}_k^-)^T + Q_k \tag{21}$$

The transformed sigma points $\chi_{k|k-1}^x$ is propagated through the measurement model to acquire measurement prediction $\hat{\mathbf{y}}_k^-$.

$$\Upsilon_{k|k-1}^x = g(\chi_{k|k-1}^x) \tag{22}$$

$$\hat{\mathbf{y}}_k^- = \sum_{i=0}^{2L} \mathbf{W}_i^{(m)} \Upsilon_{i,k|k-1}^x \tag{23}$$

$$\mathbf{P}_{\hat{y}_k \hat{y}_k} = \sum_{i=0}^{2L} \mathbf{W}_i^{(c)} (\Upsilon_{i,k|k-1}^x - \hat{\mathbf{y}}_k^-)(\Upsilon_{i,k|k-1}^x - \hat{\mathbf{y}}_k^-)^T + R_k \tag{24}$$

$$\mathbf{P}_{\hat{x}_k \hat{y}_k} = \sum_{i=0}^{2L} \mathbf{W}_i^{(c)} (\chi_{i,k|k-1}^x - \hat{\mathbf{x}}_k^-)(\Upsilon_{i,k|k-1}^x - \hat{\mathbf{y}}_k^-)^T \tag{25}$$

$$K_k = \mathbf{P}_{\hat{x}_k \hat{y}_k} \mathbf{P}_{\hat{y}_k \hat{y}_k}^{-1} \tag{26}$$

In the measurement update step, the actual system measurement y_k is used to refine prediction acquired in the time update step. The kalman gain is calculated according to (26), then the error between actual measurement y_k and predicted measurement $\hat{\mathbf{y}}_k^-$ is added to the prediction $\hat{\mathbf{x}}_k^-$. The state estimate $\hat{\mathbf{x}}_k$ and the corresponding covariance $\mathbf{P}_k^x$ can be calculated according (27) and (28).

$$\hat{\mathbf{x}}_k = \hat{\mathbf{x}}_k^- + K_k(y_k - \hat{\mathbf{y}}_k^-) \tag{27}$$

$$\mathbf{P}_k^x = \mathbf{P}_k^{x-} - K_k \mathbf{P}_{\hat{y}_k \hat{y}_k} K_k^T \tag{28}$$

The state estimate $\hat{\mathbf{x}}_k$ and covariance $\mathbf{P}_k^x$ acquired will be used in the next iteration of UKF.

IV. IMPLEMENTATION

The complete dynamics of the DFIG system given in (2) to (10) can be written in a compact form using a set of continuous-time nonlinear state-space equations as follows.

$$\dot{x} = f(x, u) + v \tag{29}$$

$$y = g(x) + w \tag{30}$$

where x is the state vector, y is the measured output, and u is the DFIG input. $v \sim \mathcal{N}(0, Q)$ and $w \sim \mathcal{N}(0, R)$ are the additive process and measurement noises, respectively. As obvious, the order of x is 18 with detail as follows.

$$x = \begin{bmatrix} V_{DC} & x_{fil} & x_{GSC} & x_{drive} & x_{ind} & x_{RSC} \end{bmatrix}^T \tag{31}$$

The vector $x_{fil} = [i_{qg} \; i_{dg}]$, $x_{GSC} = [\Phi_{V_{DC}} \; \Phi_{Q_g} \; \Phi_{i_{qg}} \; \Phi_{i_{dg}}]$, and $x_{RSC} = [\Phi_{T_e} \; \Phi_{i_{qr}} \; \Phi_{i_{dr}} \; \Phi_{Q_s}]$ denote the state vector associated to GSC filter, GSC, and RSC control dynamics, respectively. The vector $x_{drive} = [\omega_t \; \omega_r \; T_g]$ stands for the state vector associated to the drive-train dynamics and the vector $x_{ind} = [i_{qs} \; i_{ds} \; i_{qr} \; i_{dr}]$ is the state vector associated to the induction generator dynamics.

The input and output pair must be chosen carefully with the aims to allow a decentralized DSE. This can be carried out as follows. The terminal current output of DFIG i_{DFIG} which is described by Fig. 1 is selected as the system output.

$$y = \begin{bmatrix} i_{qDFIG} & i_{dDFIG} \end{bmatrix}^T = \begin{bmatrix} i_{qs} - i_{qg} & i_{ds} - i_{dg} \end{bmatrix}^T \tag{32}$$

whereas the terminal voltage v_s is set as the system input, namely

$$u = \begin{bmatrix} v_{qs} & v_{ds} \end{bmatrix}^T \tag{33}$$

This choice of input and output pair is adopted from [32] and allows for a distributed DSE framework. The advantage is that the DSE is applicable to any configurations of DFIGs, namely stand-alone or grid connected, as long as these terminal measurements are available. In order to implement DFIG state estimation using the discrete UKF discussed in section III, the continuous-time model, namely (29) and (30), needs to be transformed into its discrete-time form. We use a simple backward Euler to estimate the time derivatives. In other words, $\dot{x} = \frac{\mathbf{x}_k - \mathbf{x}_{k-1}}{\Delta t}$ where Δt is the time step. If we substitute this to (29), it yields

$$\frac{\mathbf{x}_k - \mathbf{x}_{k-1}}{\Delta t} = f(\mathbf{x}_{k-1}, \mathbf{u}_{k-1}) \tag{34}$$

Therefore, the time-continuous system (29) and (30) can be transformed into the corresponding discrete-time system form shown as follows.

$$\mathbf{x}_k = \mathbf{x}_{k-1} + (f(\mathbf{x}_{k-1}, \mathbf{u}_{k-1}) + v_{k-1})\Delta t \tag{35}$$

$$\mathbf{y}_k = g(\mathbf{x}_k) + w_k \tag{36}$$

This discretized system is in the form of (17) and (18), and hence is ready for DSE process.

The overall structure of the DFIG system and DSE using kalman filter is shown in Fig. 5. We can see that in general the DSE framework is made of two subsystems, namely the DFIG dynamic model (top left) and the state-estimator (bottom right). Both the subsystems are implemented in Matlab/Simulink. The DFIG system is simulated using the continuous-time model given in Section II, whereas the DSE is realized using the descritized system in (35) and (36), and discrete-time UKF algorithm provided in Section III. We also use the zero-order hold (ZOH) to mimic the sampling process of y and u as given in (32) and (33), respectively. The system parameter values for the entire study are shown in Appendix VI. In a basic DSE procedure, the model and the parameters are always assumed to be known. Also, the faults considered in this paper are balanced symmetrical faults. The performance of UKF estimation is evaluated by comparing the state estimation, $\hat{x}$, with the actual state, x, through simulations.

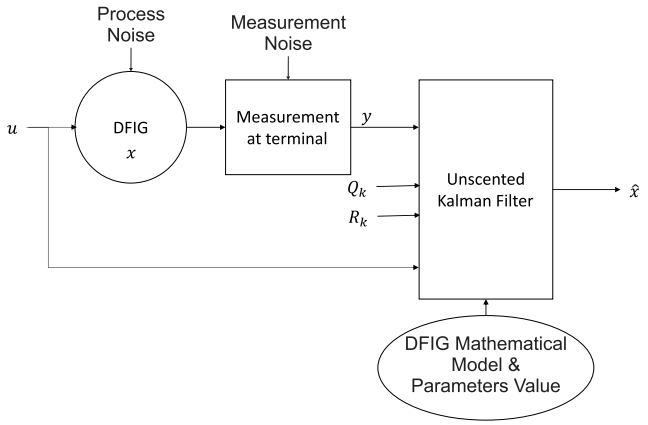

FIGURE 5. Framework of DSE for DFIG using UKF.

V. SIMULATION RESULTS

In this section, we will establish the robustness of the proposed DSE framework on the DFIG system configuration given in Fig.1. To serve this this purpose, several realistic scenarios are carefully devised.

A. STEADY-STATE PERFORMANCE

This study case focuses on evaluating the performance of the Unscented Kalman Filter (UKF) in estimating the state of DFIG under steady-state conditions. In particular, we will study the influence of initial state estimate $\hat{\mathbf{x}}_0$ on $\hat{x}$. For this purpose, three scenarios are devised as follows. Firstly, the UKF is initialized with all elements of $\hat{\mathbf{x}}_0$ set to 1. Secondly, the UKF begins with $\hat{\mathbf{x}}_0$ initialized with random elements between 0 and 1. Thirdly, the UKF uses an initialization where all elements of $\hat{\mathbf{x}}_0$ are set equal to their corresponding steady-state values.

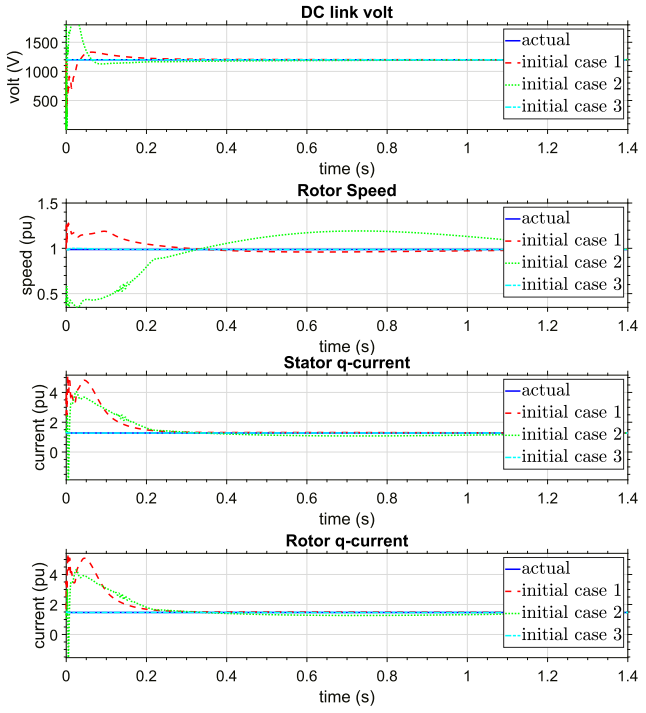

FIGURE 6. UKF state estimation for a steady-state condition.

The estimation results for these initial estimation cases are depicted in Fig. 6. Although the system is modeled with 18 state variables, the estimation results of the proposed method will only be presented for some the states in order to save space. Virtually in all cases, the estimations eventually converge towards the actual values of DFIG states in less than 0.2 seconds. Most notably, the third case, where the initial estimation matches the steady-state value, showed the best performance as expected. Despite this fact, the other two cases represent a more realistic condition as $\hat{\mathbf{x}}_0$ is generally unknown. For further analysis, the initial estimation in the third case will be used throughout the rest of this paper.

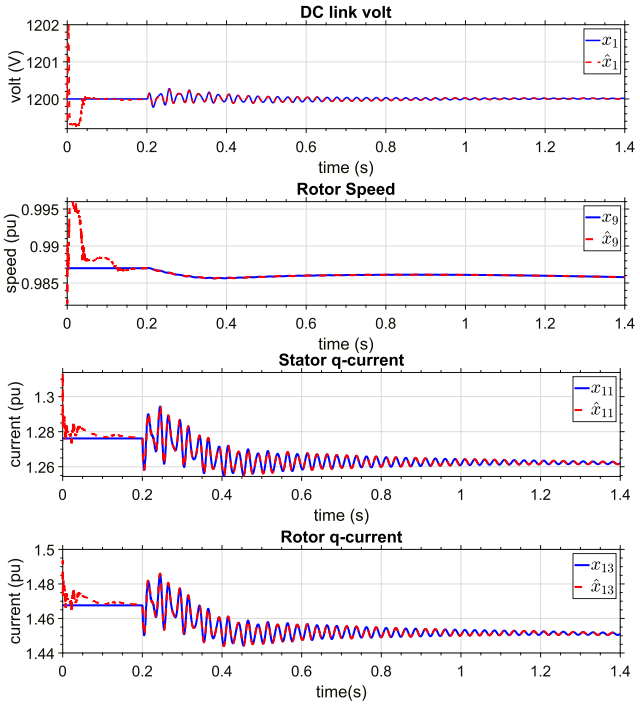

FIGURE 7. UKF state estimation during transient: noise-free case.

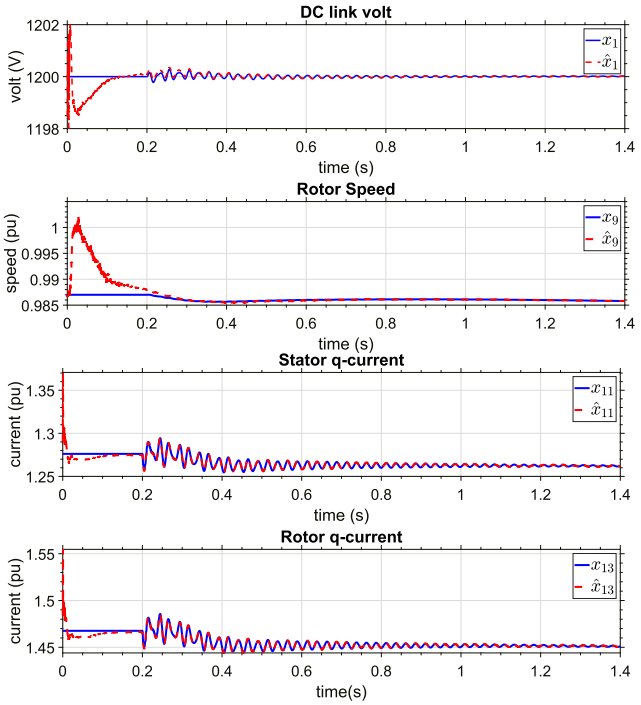

FIGURE 8. UKF state estimation during transient: noisy case.

B. TRANSIENT PERFORMANCE

In this case, we investigate the performance of UKF to estimate the DFIG states during a transient condition. To simulate the case, the DFIG system Initially operates in steady-state. At $t = 0.2\ s$, the mechanical torque T_m working on the wind turbine suddenly decreases by 2%, and at the same time there is a sudden increase in the infinite bus voltage E_b by 1%. The system will experience a transient period in response to these disturbances and UKF is tested to track DFIG states. We will simulate the estimation results for both the noise-free and noisy conditions.

The results of state estimate for the noise-free condition is shown in Fig. 7. In the absence of noise, the UKF is able to produce generally good estimates and track the actual state very accurately, although initially the estimates were quite erroneous.

Furthermore, the state estimate for the noisy condition is provided in Fig. 8. This scenario is carried out by adding a normally distributed process noise with mean and covariance 0 and $Q_k = 10^{-12} I_{18}$, respectively, and a normally distributed measurement noise with mean and covariance 0 and $R_k = 10^{-5} I_2$, respectively. I_n stands for the $n \times n$ identity matrix. The UKF is generally be able to emulate the states of DFIG with a high degree of accuracy, even with the presence of both process and measurement noises. Comparing to the noise-free case, as expected, it is also visible that UKF estimation takes a longer time to converge to the actual states when the noises are present in the system, indicating the challenge for the DFIG state estimation during noise conditions.

C. DIFFERENT LEVEL OF PROCESS NOISE

This case investigates the results of UKF estimation under different levels of process noise. With the aim to demonstrate this, the simulation is performed by adding the noise with different covariance values which are varied as follows: $Q_k = 10^{-16} I_{18}, 10^{-12} I_{18}$, and $10^{-8} I_{18}$. On the other hand, the measurement noise covariance remains constant at $R_k = 10^{-6} I_2$.

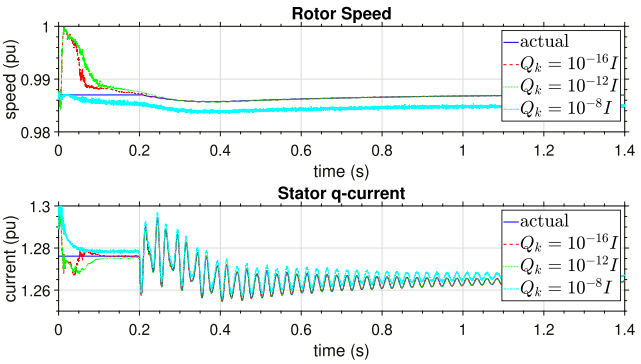

FIGURE 9. UKF state estimation for different process noise level.

Fig. 9 depicts the performance of UKF under these scenarios. As expected, it is visible that state estimator produces more accurate outcomes as the covariance becomes smaller. On the other hand, the state estimates results in more erroneous outputs or even biased estimates due to the presence of high-level of noise. This circumstance is evident for the case with $Q_k = 10^{-8} I_{18}$. Hence, it can be concluded that UKF produces a better estimate of DFIG states when the system is subjected to a sufficiently small process noise.

D. DIFFERENT LEVEL OF MEASUREMENT NOISE

In this scenario, we investigate the accuracy of UKF when different level of noise is present in the measurement. This is carried out by varying the covariance related to the measurement noise R_k. For this, three scenarios of measurement noise are devised as follows: $R_k = 10^{-6}I_2, 10^{-4}I_2, 10^{-2}I_2$, while the process noise covariance is held constant at $Q_k = 10^{-16}I_{18}$ for all cases.

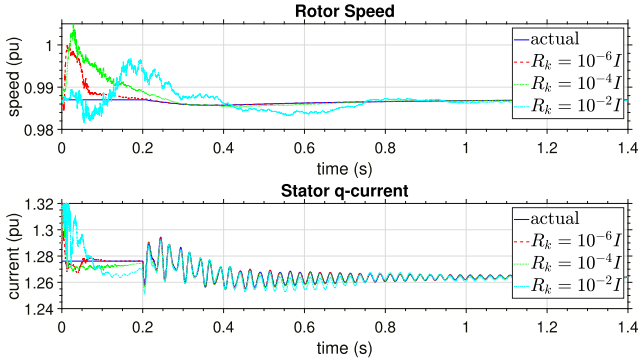

FIGURE 10. UKF state estimation for different measurement noise level.

Fig. 10 illustrate the performance of UKF under these conditions. It is visible that UKF algorithm is eventually able to track the actual states even when the system is subjected to a large measurement noise covariance. Different from the case of process noise, UKF can produce unbiased state estimates in virtually all scenarios. It is also to be noted that UKF require a longer time to converge to the actual states for larger measurement noises as clearly visible in Fig. 10.

E. LOW VOLTAGE RIDE THROUGH (LVRT)

One of the grid codes of modern power systems requires the DIFG to remain connected to the grid in the event of a significant drop in the terminal voltage. This is known as low voltage ride through (LVRT) [33]. In this scenario, we investigate the ability of UKF-based DSE during LVRT. For this purpose, we simulate a significant voltage drop at E_b and in response to this, the terminal voltage of DFIG will also undergo a significant voltage drop. Three cases are constructed for this purpose, namely case-1 (60%), case-2 (70%), and case-3 (80%). In all the cases, the DFIG initially operates in steady-state, then at $t = 0.2\ s$, the infinite bus voltage suddenly drops by the amount according to each scenario

The estimation results for the three cases is presented in Figs. 11 and 12. It is obvious beforehand that the DFIG system exhibits a strong nonlinearity for all cases. Despite this, UKF estimates and tracks the DFIG states with a high-degree of precision. Also, the state estimate produces only a slightly more erroneous outcomes as the voltage drop become more severe. This phenomenon highlights that UKF-based state estimator maintains the robustness even during severe faults, which may be essential for monitoring and control purposes of DFIGs

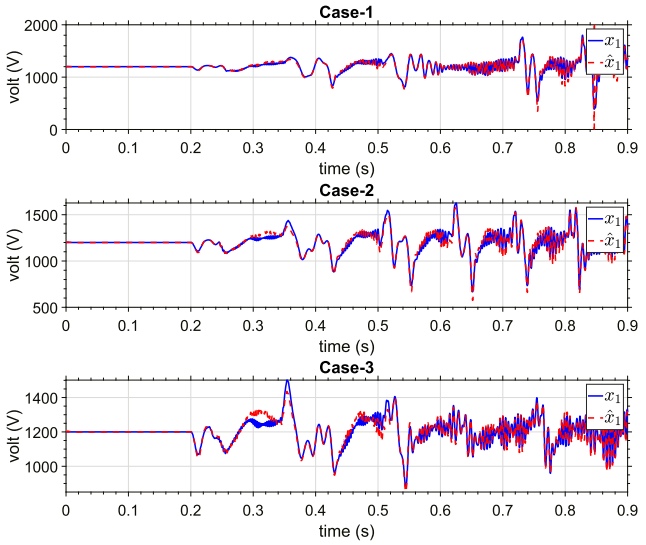

FIGURE 11. UKF DC link voltage estimation during LVRT.

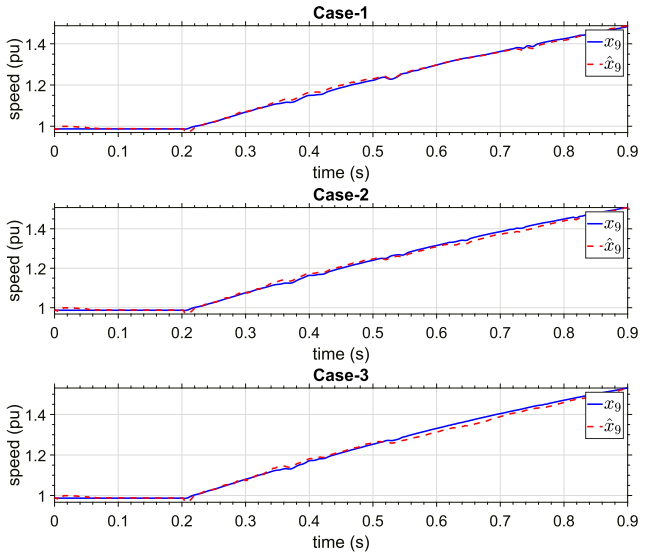

FIGURE 12. UKF rotor speed estimation during LVRT.

F. UNKNOWN INPUTS

In this case, some of the previously known constant inputs, namely, Q_{sref}, Q_{gref}, and V_{DCref}, are treated as the unknown inputs. See Figs. 2 and 3 to locate these control inputs. The goal is to perform state estimate together with the unknown inputs. It can be done by augmenting those unknown inputs into the state vector (31), and hence the extended state space equations become as follows.

$$\dot{x}_{UI} = f_{UI}(x_{UI}, u_{UI}) + v_{UI} \tag{37}$$

where $x_{UI} = \begin{bmatrix} x & Q_{sref} & V_{DCref} & Q_{gref} \end{bmatrix}^T$. $f_{UI} = \begin{bmatrix} f & 0 & 0 & 0 \end{bmatrix}^T$ with f equal to (29). The state equations pertinent to the unknown inputs are equal to zero as they remain constant throughout the study period. With this, we can proceed to the UKF procedure as in the previous cases.

We then perturb the system using the same fault used in Section V-B. The results for the unknown inputs

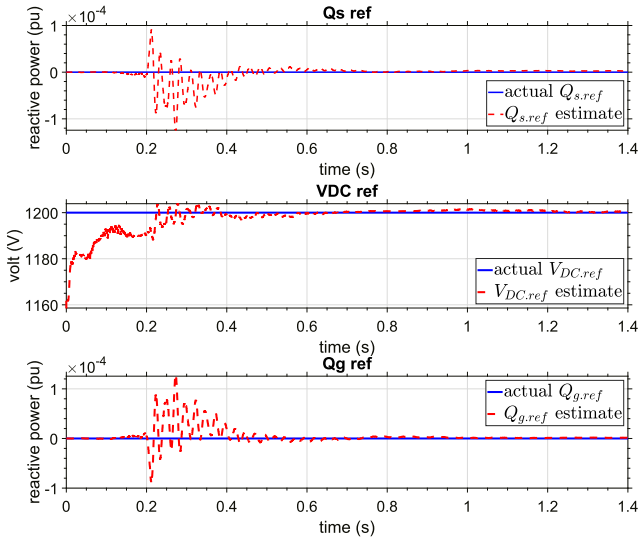

FIGURE 13. UKF unknown input estimation.

Q_{sref}, V_{DCref}, and Q_{gref} are provided in Fig. 13. It can be observed that generally UKF is able to produce a high degree estimate of the unknown inputs. Although UKF initially fails to estimate the unknown input prior to $t = 0.5\ s$, it is eventually able to track the unknown inputs very accurately.

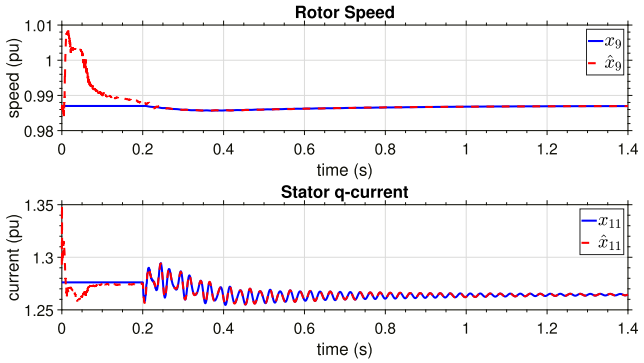

FIGURE 14. UKF state estimation with unknown inputs.

Fig. 14 illustrates DFIG state estimation output while the unknown inputs are also estimated simultaneously. It is evident that UKF can still provide an accurate estimates of the states during the unfavorable conditions of missing inputs measurements. This shows that by treating the unknown inputs in the extended states as given in (37), UKF is capable of providing accurate estimations for both the states and the unknown inputs.

VI. CONCLUSION

This paper has demonstrated the robustness of UKF-based DSE on a high-order DFIG model with 18 states. The simulation results show that UKF is capable of producing accurate estimations of DFIG states under steady-state and transient conditions, and the LVRT as well as different noisy conditions. It has been observed that UKF method is less sensitive to the measurement noise than process noise, as demonstrated by the simulation results that shows UKF is able to maintain an accurate estimates under higher measurement noise but results in inaccurate results under higher process noise. Moreover, it has been demonstrated that UKF produces reasonably good estimations even with the unknown inputs. UKF is able to emulate the states of the DFIG and the unknown inputs simultaneously. UKF has also proved the robustness by consistently estimating DFIG states accurately across different scenarios in simulations, showcasing its reliability in diverse adverse conditions. Further research could concentrate on real-time validation by employing sensors to measure accessible states.

APPENDIX
SYSTEM PARAMETERS

See Table 1.

TABLE 1. System parameters.

DFIG Parameters			
P rated	100 MW	V_{DC} rated	1200 V
X_s	4.0451 pu	ω_b	$2\pi \times 50$
X_m	3.95279 pu	$C_{V_{DC}}$	$50 \times 14000\mu F$
X_r	4.0523 pu	X_g	0.3 pu
r_s	0.00488 pu	r_r	0.00549 pu
K_{tg}	0.15	D_{tg}	1.5
H_t	4.29	D_g	0
H_g	0.9	D_t	0
K_{pT_e}	0	K_{iT_e}	14.3
K_{pQ_s}	0	K_{iQ_s}	26
K_{pi_r}	0.06	K_{ii_r}	0.55
$K_{pV_{DC}}$	-0.0036	$K_{iV_{DC}}$	-0.13
K_{pQ_g}	0	K_{iQ_g}	31
K_{pi_g}	0.6	K_{ii_g}	9.55
Series Compensated Line Parameters			
Base MVA	100 MVA	X_C	0.025 pu
R_L	0.02 pu	X_L	0.5 pu

REFERENCES

[1] Y. Ding, C. Singh, L. Goel, J. Østergaard, and P. Wang, "Short-term and medium-term reliability evaluation for power systems with high penetration of wind power," *IEEE Trans. Sustain. Energy*, vol. 5, no. 3, pp. 896–906, Jul. 2014.

[2] S. S. Yu, J. Guo, T. K. Chau, T. Fernando, H. H. Iu, and H. Trinh, "An unscented particle filtering approach to decentralized dynamic state estimation for DFIG wind turbines in multi-area power systems," *IEEE Trans. Power Syst.*, vol. 35, no. 4, pp. 2670–2682, Jul. 2020.

[3] E. Vittal, M. O'Malley, and A. Keane, "A steady-state voltage stability analysis of power systems with high penetrations of wind," *IEEE Trans. Power Syst.*, vol. 25, no. 1, pp. 433–442, Feb. 2010.

[4] X. Liu, Y. Liu, J. Liu, Y. Xiang, and X. Yuan, "Optimal planning of AC-DC hybrid transmission and distributed energy resource system: Review and prospects," *CSEE J. Power Energy Syst.*, vol. 5, no. 3, pp. 409–422, Sep. 2019.

[5] W. Tang, J. Hu, Y. Chang, and F. Liu, "Modeling of DFIG-based wind turbine for power system transient response analysis in rotor speed control timescale," *IEEE Trans. Power Syst.*, vol. 33, no. 6, pp. 6795–6805, Nov. 2018.

[6] F. Mei. (2008). *Small-Signal Modelling and Analysis of Doubly-Fed Induction Generators in Wind Power Applications*. [Online]. Available: https://spiral.imperial.ac.uk/handle/10044/1/4249

[7] O. P. Mahela, N. Gupta, M. Khosravy, and N. Patel, "Comprehensive overview of low voltage ride through methods of grid integrated wind generator," *IEEE Access*, vol. 7, pp. 99299–99326, 2019.

[8] L. Fan, H. Yin, and Z. Miao, "On active/reactive power modulation of DFIG-based wind generation for interarea oscillation damping," *IEEE Trans. Energy Convers.*, vol. 26, no. 2, pp. 513–521, Jun. 2011.

[9] R. Liu, J. Yao, X. Wang, P. Sun, J. Pei, and J. Hu, "Dynamic stability analysis and improved LVRT schemes of DFIG-based wind turbines during a symmetrical fault in a weak grid," *IEEE Trans. Power Electron.*, vol. 35, no. 1, pp. 303–318, Jan. 2020, doi: 10.1109/TPEL.2019.2911346.

[10] Z. Rafiee, R. Heydari, M. Rafiee, M. R. Aghamohammadi, and F. Blaabjerg, "Enhancement of the LVRT capability for DFIG-based wind farms based on short-circuit capacity," *IEEE Syst. J.*, vol. 16, no. 2, pp. 3237–3248, Jun. 2022.

[11] Y. Cui, R. G. Kavasseri, and S. M. Brahma, "Dynamic state estimation assisted out-of-step detection for generators using angular difference," *IEEE Trans. Power Del.*, vol. 32, no. 3, pp. 1441–1449, Jun. 2017.

[12] J. Zhao, M. Netto, Z. Huang, S. S. Yu, A. Gómez-Expósito, S. Wang, I. Kamwa, S. Akhlaghi, L. Mili, V. Terzija, A. P. S. Meliopoulos, B. Pal, A. K. Singh, A. Abur, T. Bi, and A. Rouhani, "Roles of dynamic state estimation in power system modeling, monitoring and operation," *IEEE Trans. Power Syst.*, vol. 36, no. 3, pp. 2462–2472, May 2021.

[13] J. Zhao, A. Gómez-Expósito, M. Netto, L. Mili, A. Abur, V. Terzija, I. Kamwa, B. Pal, A. K. Singh, J. Qi, Z. Huang, and A. P. S. Meliopoulos, "Power system dynamic state estimation: Motivations, definitions, methodologies, and future work," *IEEE Trans. Power Syst.*, vol. 34, no. 4, pp. 3188–3198, Jul. 2019.

[14] Y. Liu, A. K. Singh, J. Zhao, A. P. S. Meliopoulos, B. Pal, M. A. M. Ariff, T. van Cutsem, M. Glavic, Z. Huang, I. Kamwa, L. Mili, A. S. Mir, A. Taha, V. Terzija, and S. Yu, "Dynamic state estimation for power system control and protection," *IEEE Trans. Power Syst.*, vol. 36, no. 6, pp. 5909–5921, Nov. 2021.

[15] E. Ghahremani and I. Kamwa, "Local and wide-area PMU-based decentralized dynamic state estimation in multi-machine power systems," *IEEE Trans. Power Syst.*, vol. 31, no. 1, pp. 547–562, Jan. 2016.

[16] E. Ghahremani and I. Kamwa, "Online state estimation of a synchronous generator using unscented Kalman filter from phasor measurements units," *IEEE Trans. Energy Convers.*, vol. 26, no. 4, pp. 1099–1108, Dec. 2011.

[17] X. Bai, F. Qin, L. Ge, L. Zeng, and X. Zheng, "Dynamic state estimation for synchronous generator with communication constraints: An improved regularized particle filter approach," *IEEE Trans. Sustain. Comput.*, vol. 8, no. 2, pp. 222–231, Feb. 2022.

[18] H. Liu, F. Hu, J. Su, X. Wei, and R. Qin, "Comparisons on Kalman-filter-based dynamic state estimation algorithms of power systems," *IEEE Access*, vol. 8, pp. 51035–51043, 2020.

[19] Y. Cui and R. Kavasseri, "A particle filter for dynamic state estimation in multi-machine systems with detailed models," *IEEE Trans. Power Syst.*, vol. 30, no. 6, pp. 3377–3385, Nov. 2015.

[20] S.-H. Hur, "Estimation of useful variables in wind turbines and farms using neural networks and extended Kalman filter," *IEEE Access*, vol. 7, pp. 24017–24028, 2019.

[21] S. Yu, T. Fernando, K. Emami, and H. H. Iu, "Dynamic state estimation based control strategy for DFIG wind turbine connected to complex power systems," *IEEE Trans. Power Syst.*, vol. 32, no. 2, pp. 1272–1281, Mar. 2017.

[22] Z. Cao and X. Du, "An intelligent optimization-based particle filter for fault diagnosis," *IEEE Access*, vol. 9, pp. 87839–87848, 2021.

[23] S. Yu, T. Fernando, H. H. Iu, and K. Emami, "Realization of state-estimation-based DFIG wind turbine control design in hybrid power systems using stochastic filtering approaches," *IEEE Trans. Ind. Informat.*, vol. 12, no. 3, pp. 1084–1092, Jun. 2016.

[24] W. Sheng, H. Zhang, K. -Y. Liu, and X. Meng, "An unscented particle filter algorithm towards data quality improvement in sustainable distribution power systems," *CSEE J. Power Energy Syst.*, early access, Sep. 8, 2023, doi: 10.17775/CSEEJPES.2020.05010.

[25] G. Anagnostou and B. C. Pal, "Derivative-free Kalman filtering based approaches to dynamic state estimation for power systems with unknown inputs," *IEEE Trans. Power Syst.*, vol. 33, no. 1, pp. 116–130, Jan. 2018.

[26] Z. Zheng, J. Zhao, L. Mili, Z. Liu, and S. Wang, "Unscented Kalman filter-based unbiased minimum-variance estimation for nonlinear systems with unknown inputs," *IEEE Signal Process. Lett.*, vol. 26, no. 8, pp. 1162–1166, Aug. 2019.

[27] G. Anagnostou, L. P. Kunjumuhammed, and B. C. Pal, "Dynamic state estimation for wind turbine models with unknown wind velocity," *IEEE Trans. Power Syst.*, vol. 34, no. 5, pp. 3879–3890, Sep. 2019.

[28] A. R. Ramadhan, H. R. Ali, and R. Irnawan, "Dynamic state estimation of doubly-fed induction generator (DFIG) using unscented Kalman filter method," B.E. Thesis, Univ. Gadjah Mada, Yogyakarta, IN, USA, 2023.

[29] L. Fan, R. Kavasseri, Z. L. Miao, and C. Zhu, "Modeling of DFIG-based wind farms for SSR analysis," *IEEE Trans. Power Del.*, vol. 25, no. 4, pp. 2073–2082, Oct. 2010.

[30] S. J. Julier and J. K. Uhlmann, "Unscented filtering and nonlinear estimation," *Proc. IEEE*, vol. 92, no. 3, pp. 401–422, Mar. 2004.

[31] E. A. Wan and R. Van Der Merwe, "The unscented Kalman filter for nonlinear estimation," in *Proc. IEEE Adapt. Syst. Signal Process., Commun., Control Symp.*, Oct. 2000, pp. 153–158.

[32] A. K. Singh and B. C. Pal, "Decentralized dynamic state estimation in power systems using unscented transformation," *IEEE Trans. Power Syst.*, vol. 29, no. 2, pp. 794–804, Mar. 2014.

[33] Y. M. Alsmadi, L. Xu, F. Blaabjerg, A. J. P. Ortega, A. Y. Abdelaziz, A. Wang, and Z. Albataineh, "Detailed investigation and performance improvement of the dynamic behavior of grid-connected DFIG-based wind turbines under LVRT conditions," *IEEE Trans. Ind. Appl.*, vol. 54, no. 5, pp. 4795–4812, Sep. 2018.

ALIF RAVI RAMADHAN received the B.Eng. degree in electrical engineering from Universitas Gadjah Mada (UGM), Yogyakarta, Indonesia, in 2023. He is currently an Assistant Researcher with the Transmission and Distribution Laboratory, UGM. His research interest includes power system dynamics stability and control.

HUSNI ROIS ALI (Senior Member, IEEE) received the B.Eng. degree in electrical engineering from Universitas Gadjah Mada (UGM), Yogyakarta, Indonesia, in 2009, the M.Eng. degree in electrical engineering from Chulalongkorn University, Bangkok, Thailand, in 2013, and the Ph.D. degree in electrical engineering from the Department of Electrical and Electronic Engineering, Imperial College London, London, U.K. He is currently an Assistant Professor with the Department of Electrical and Information Engineering (DTETI), UGM. His research interests include power system dynamics stability and control, and wind farm modeling. He is an Associate Editor of *Journal of Modern Power Systems and Clean Energy* and IEEE Open Access Journal of Power and Energy.

RONI IRNAWAN (Senior Member, IEEE) received the bachelor's (S.T.) degree in electrical engineering from Universitas Gadjah Mada (UGM), Indonesia, in 2007, the M.Sc. degree in electric power engineering from the Chalmers University of Technology, Sweden, in 2011, and the Ph.D. degree in energy technology from Aalborg University, Denmark, in 2019. From 2012 to 2015, he was an HVdc Modeling and Simulation Engineer with ABB AB, Sweden. He is currently a Lecturer with the Department of Electrical and Information Engineering, UGM, and a Senior Electrical Engineer (part-time) with Merz Consulting, Australia. He was a recipient of the 2020 CIGRE Thesis Award for the Ph.D. thesis entitled "Planning and control of expandable multi-terminal VSC-HVDC transmission systems." His Ph.D. thesis was also published by Springer as part of the "Springer Theses" book series, which recognizes outstanding Ph.D. research around the world.